Solar Energy 153 (2017) 262–275

Contents lists available at ScienceDirect

Solar Energy

journal homepage: www.elsevier.com/locate/solener

Modeling and analysis of a smart grid monitoring system for renewable energy sources

Yasin Kabalci [a,*], Ersan Kabalci [b]

[a] Department of Electrical and Electronics Engineering, Faculty of Engineering, Omer Halisdemir University, 51240 Nigde, Turkey
[b] Department of Electrical and Electronics Engineering, Faculty of Engineering and Architecture, Nevsehir HBV University, 50300 Nevsehir, Turkey

ARTICLE INFO

Article history:
Received 21 November 2016
Received in revised form 15 May 2017
Accepted 20 May 2017

Keywords:
Renewable energy
Smart grid
Power line communication
Microgrid
Remote monitoring

ABSTRACT

The observing and metering processes are necessary in renewable energy conversion systems as applied in smart grid applications of conventional grid. In this study, the requirements of the renewable energy sources examined with a solar microgrid model that is developed via Matlab/Simulink. The dc-ac conversion system utilized in this paper contains three solar power plants with maximum power point tracking (MPPT) system and a multilevel inverter to create three-phase ac line voltages. The transmission line is modeled at the output of the inverter with a length of 25 km by using real line parameters. The infrastructure of power line communication (PLC) is managed by binary phase shift keying (BPSK) modems that are located in different places. The usage of the proposed energy monitoring technique eliminates additional monitoring costs due to the fact that the power lines are not only exploited to carry the generated voltage, but also utilized to convey the drawn power rate of loads at the back-end of the microgrid.

1. Introduction

The microgrid is defined as a small autonomous system that is constituted with combining several distributed energy sources such as solar, wind, fuel cells, biomass, and so on together. The distributed generation (DG) systems based on renewable energy sources demonstrate a rapid emerging. Small scale power generators in the level of medium and low-voltage power systems can be established by the DG systems. Therefore, smart grid (SG) systems are important parts of the DG systems. The SG applications include two main infrastructures that are smart transmission grid (STG) and smart distribution grid (SDG). The emerging smart grid systems require sensing of data from all the sensors located on the system within a few power cycles (Kabalci et al., 2012; Ginot et al., 2010; Kurohane et al., 2010; Zhang et al., 2010). The power line communication (PLC) term is exploited to describe transmitting and receiving process of any type data over the conventional transmission lines. This notion also defines the main framework of the smart grid. The usage of power lines as a transmission medium prevents the supplementary establishment costs to get the systems communicated together. The PLC applications allow data rates of transmission as much as 200 Mbps using single phase with 220 V/50 Hz (Mannah et al., 2011; Kosonen and Ahola, 2010; Son et al., 2010; Tsuzuki, 2006; Lin et al., 2009).

The most studied area of the renewable energy sources is the use of the PVs since generating energy via solar energy sources offers several advantages such as precluding air pollution, soundless operation in consequence of the motionless, and reduced maintenance costs. Although the PVs are frequently assumed as a costly process to generate electrical energy, the most appropriate solution to supply the required energy is the usage of standalone PV applications. In grid connected systems, voltage source inverters (VSI) capable of pulse-width modulation (PWM) are generally employed to connect renewable energy sources and the grid. In addition, the current control is an important feature of this type converter to supply high quality power to the utility grid. When the cost of the grid connected systems is considered, the cost can be reduced by employing fewer power conversion stages and components (Kabalci and Kabalci, 2010; Kabalci, 2013; Kabalci, 2015; Ma et al., 2013).

Several remote monitoring methods in terms of energy monitoring, weather monitoring and fault detection systems have been proposed for both traditional and renewable energy sources (Wilkinson et al., 2014; Almas et al., 2014; Ahmed et al., 2016; Padilla et al., 2014; Silvestre et al., 2013; Kamel et al., 2015; Vanfretti et al., 2016; Senthilnathan and Annapoorani, 2016; Venkatraman et al., 2016; Silva et al., 2017; Tina and Grasso, 2014; Shariff et al., 2013; Gaurav et al., 2014; Kabalci et al.,

* Corresponding author.
E-mail addresses: yasinkabalci@ohu.edu.tr (Y. Kabalci), kabalci@nevsehir.edu.tr (E. Kabalci).

http://dx.doi.org/10.1016/j.solener.2017.05.063
0038-092X/

2016; Fateh et al., 2013; Madueño et al., 2016; Cabanas et al., 2007; Mohamed et al., 2014; Shariff et al., 2015; Tung et al., 2014; Chi et al., 2016; Collotta and Pau, 2015; Le et al., 2016; Fabrizio et al., 2017; Harid et al., 2016; Atalik et al., 2014; Zaker et al., 2014) so far. When the studies related to the remote monitoring are examined, it is clearly seen that these systems can be classified as wired, wireless and hybrid remote monitoring systems. Remote monitoring systems utilizing wired communication infrastructure cover Supervisory Control and Data Acquisition (SCADA) (Wilkinson et al., 2014; Almas et al., 2014) and Ethernet-based systems (Ahmed et al., 2016; Padilla et al., 2014; Silvestre et al., 2013; Kamel et al., 2015; Vanfretti et al., 2016; Senthilnathan and Annapoorani, 2016; Venkatraman et al., 2016; Silva et al., 2017; Tina and Grasso, 2014). Wireless remote monitoring systems widely utilize GSM (GPRS, 3G or LTE), ZigBee or Bluetooth systems (Shariff et al., 2013; Gaurav et al., 2014; Kabalci et al., 2016; Fateh et al., 2013; Madueño et al., 2016; Cabanas et al., 2007; Mohamed et al., 2014; Shariff et al., 2015; Tung et al., 2014; Chi et al., 2016; Collotta and Pau, 2015; Le et al., 2016; Fabrizio et al., 2017; Harid et al., 2016). In addition, few systems associated with wired systems and wireless communication systems, for instance combining fiber or Ethernet systems with wireless methods exist (Venkatraman et al., 2016; Atalik et al., 2014; Zaker et al., 2014). While a remote monitoring system based on SCADA for observing status of the various parameters of wind turbines are investigated in Wilkinson et al. (2014), a phase measurement unit (PMU) for a laboratory is considered by open source SCADA system in Almas et al. (2014). Ahmed et al. (2016) investigated an Ethernet based optical communication system for small scale wind turbine farms. In another study, in Padilla et al. (2014), authors aimed to provide a remote monitoring, control and protection system for electrical power systems. In addition, several remote monitoring and fault detection systems based on Ethernet communication protocol are considered in Kamel et al. (2015), Vanfretti et al. (2016), Tina and Grasso (2014).

On the other hand, a large part of wireless communication systems exploited for remote monitoring are concentrated on using of the GSM protocols (Shariff et al., 2013; Gaurav et al., 2014; Kabalci et al., 2016; Fateh et al., 2013; Madueño et al., 2016; Cabanas et al., 2007; Mohamed et al., 2014). A GSM based remote monitoring system by employing several sensor structures is proposed for photovoltaic energy generation systems in Shariff et al. (2013). A different GSM system is examined for both solar and wind energy generation systems in Gaurav et al. (2014). Kabalci et al. (2016) proposed a remote monitoring system for solar irrigation systems thanks to GSM and internet based communication. Other GSM based works (Fateh et al., 2013; Madueño et al., 2016; Cabanas et al., 2007; Mohamed et al., 2014) are focused on for monitoring of transmission lines and electrical power systems in terms of leakage, fault detection and partial discharge. The most widely utilized wireless communication method rather than the GSM based systems is ZigBee communication systems. A wireless remote monitoring system based on ZigBee communication protocol to observe grid connected PV systems is reported in Shariff et al. (2015). While Tung et al. (2014) proposed an AMI system for high-rise buildings, Chi et al. (2016) reported another AMI system for high-traffics smart metering by exploiting ZigBee communication system. In (Collotta and Pau (2015), authors studied for a measurement and energy management system that is originated from Bluetooth low energy. A monitoring and fault detection system for photovoltaics in which Bluetooth data transmission method is utilized is reported in Le et al. (2016). Apart from these studies, there are some studies related to wireless sensor networks (WSN) (Fabrizio et al., 2017) and wireless local area network (WLAN) (Harid et al., 2016) for energy demand issue and leakage current detection, respectively.

The conducted literature review is obviously showed that the remote monitoring systems are generally based on either wired communication systems utilizing fiber and Ethernet or wireless communication systems using GSM, ZigBee and Bluetooth. Even though energy monitoring or remote monitoring systems can be accomplished by employing these mentioned different communication protocols, these energy-monitoring methods come up with a significant amount of additional cost. On the other hand, there is a significant gap in the literature about usage of power lines as a communication medium both for remote monitoring and for AMI applications. In this study, a new method to eliminate this expense is proposed in which the conventional electrical power lines are not only exploited to transmit the generated electricity, but also exploited to carry the measurements of solar plants located in different places. Therefore, the main aim of this study is to contribute at this point to the literature by considering power lines as an alternative communication medium for remote monitoring applications of the smart grids. In addition, this proposed method provides several significant advantages such as eliminating channel installation cost, ability to use existing power lines more efficiently and the possibility of different channel environments that do not require obtaining license and possibility to create smart grid infrastructure.

The outline of this paper is as follows: Section 2 describes the designed distributed generation and energy conversion stage, and the designed PLC modems are presented in Section 3. The measurement and analysis results of the proposed system are given in Section 4, and finally, conclusions are drawn in Section 5.

2. Generation and energy conversion stages

The modeled microgrid structure comprised by generation, energy conversion, transmission and monitoring stages is illustrated in Fig. 1. It is clear that the structure of the microgrid is associated with microgrid loads at the end of the transmission line. Three separate solar farms placed in different locations are taken into account in the electricity generation part of this study. The modeled solar plants cover solar arrays and strings of 150 solar panels at each solar plant that are controlled with regular Perturb and Observe (P&O) maximum power point tracking (MPPT) algorithm. The output voltage of each solar plant are regulated by buck converters and supplied to five-level diode clamped multilevel inverter (MLI) that is controlled with PI regulator and phase disposition sinusoidal pulse width modulation (PD-SPWM) algorithm. The sections of generation and energy conversion stages are introduced in the following subsections.

2.1. Solar plants and DC conversion

The voltage and current parameters of the modeled solar panels are adjusted regarding to NE-170UC1 Sharp PV panel that provides maximum power out around 170 W (NE-170UC1 Multipurpose Module, 2008). The voltage-current (V-I) and voltage-power (V-P) analysis of the modeled PV module is shown in Fig. 2 where irradiation is changed up to 1000 W/m^2 by 200 W/m^2 steps while temperature is stable at 25 °C.

The obtained curves clearly verify that the modeled PV module is perfect agreement with the PV module of the Sharp. Moreover, the modeled solar panel infrastructure can be also used to set several parameters such as open circuit voltage (V_{OC}), maximum power voltage (V_{MP}), short circuit current (I_{SC}), and maximum power current (I_{MP}) for any type of PV module. The designed solar plant models produce rated power at 25.5 kW.

The solar plants are tested by applying various irradiation values assuming all are located at geographically spanned areas.

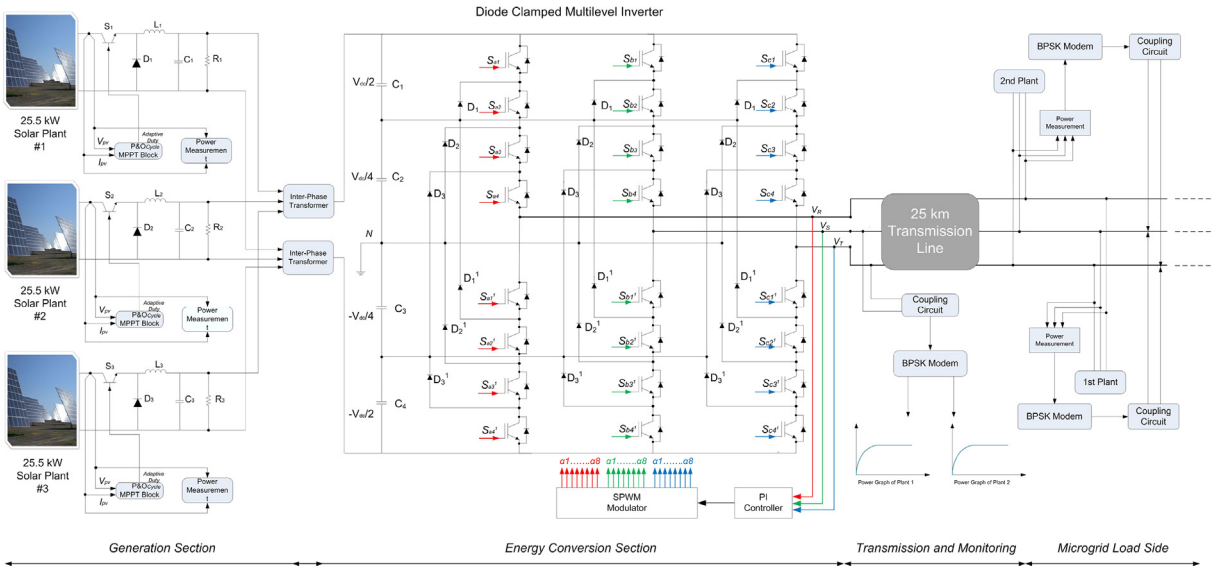

Fig. 1. The block diagram of the modeled microgrid.

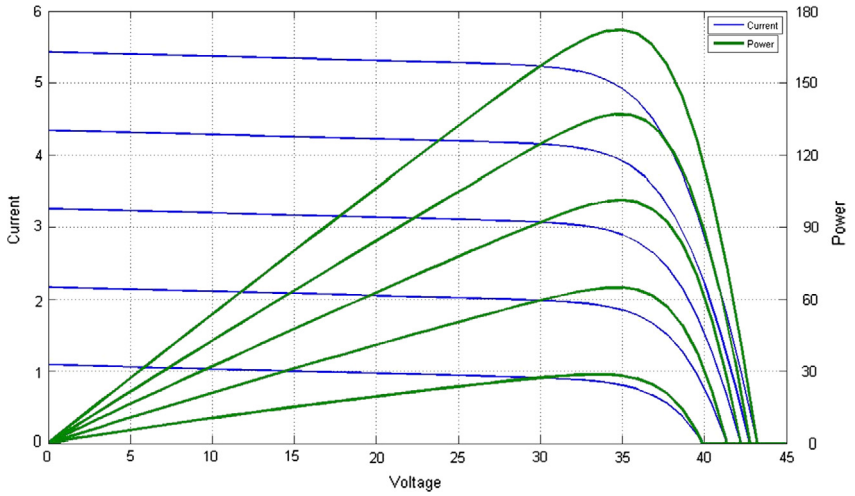

Fig. 2. I-V and P-V characteristics of the modeled PV module (irradiation increases from 200 W/m^2 to 1000 W/m^2).

Therefore, the output voltage of each plant are regulated by a buck converter that is controlled with a regular P&O MPPT algorithm allowing to obtain output voltage around 480–520 V at the dc bus outputs where it is intended to be set at 500 V. The performed analysis results are depicted in Fig. 3 where each solar plant voltages are shown respectively. The dc busbar voltage where the solar plant outputs are coupled and applied to inverter is shown in the 4th axis around 500 V. The maximum output power available at the dc busbar output is measured around 75 kW as seen in the last curve of the figure.

2.2. Energy conversion section

The coupled dc bus voltage is applied to MLI that is implemented in diode clamped five-level topology. The phase legs and controllers are illustrated in Fig. 4 where R-phase is shown with circuit and block diagrams. The advantage of diode clamped MLI topology is eliminating the separate dc source requirement at each phase leg or at each cascaded bridge cells. The dc input voltage is shared to five voltage levels by the dc capacitors on the common dc bus. The connection of C_2 and C_3 capacitors comprises the neutral point of MLI. Furthermore, the voltage at each capacitor is at $V_{dc}/4$ level that generates the five-level line voltage. The voltage stress on each switching device is limited to V_{dc} through the clamping diodes that have been named as $D_{1\ldots3}$ and $D^1_{1\ldots3}$ in this topology. The clamping diodes provide the staircase output level against to conventional full-bridge or two-level inverter. The switching orders of any phase leg to generate staircase voltage synthetize that have been analyzed for R-phase voltage V_{RN} are listed in Table 1 (Çolak et al., 2011). The four switches (S_{a1}–S_{a4}) of eight in a phase leg should be switched on at any interval to generate $V_{dc}/2$ voltage level. In the next switching interval, the switches from S_{a2} to S^1_{a1} are switched to generate $V_{dc}/4$ voltage level. The remaining switching states that constitute zero and negative outputs are repeated in the order given in Table 1.

The generated line voltages are compared by a PI controller in the modulator block seen on the right hand-side of Fig. 4. This conventional controller where the parameters are detected referring to Ziegler-Nichols method is used to limit the output voltage and power by adjusting the duty cycle of switching signals to ensure the output phase voltages at 230V_{rms} yielding line voltages around 380 V_{rms}.

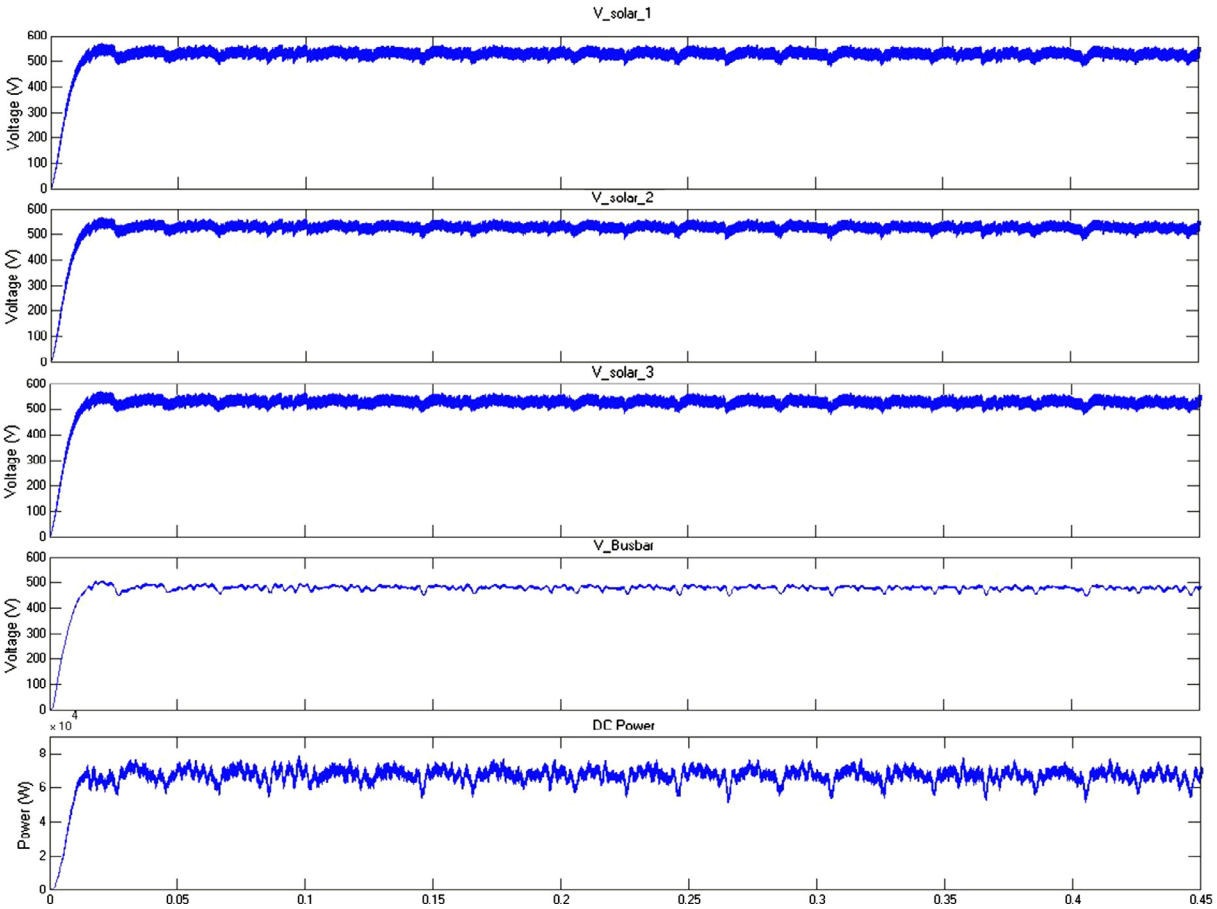

Fig. 3. DC output voltages of the solar plants, bus bar voltage, and DC power graph.

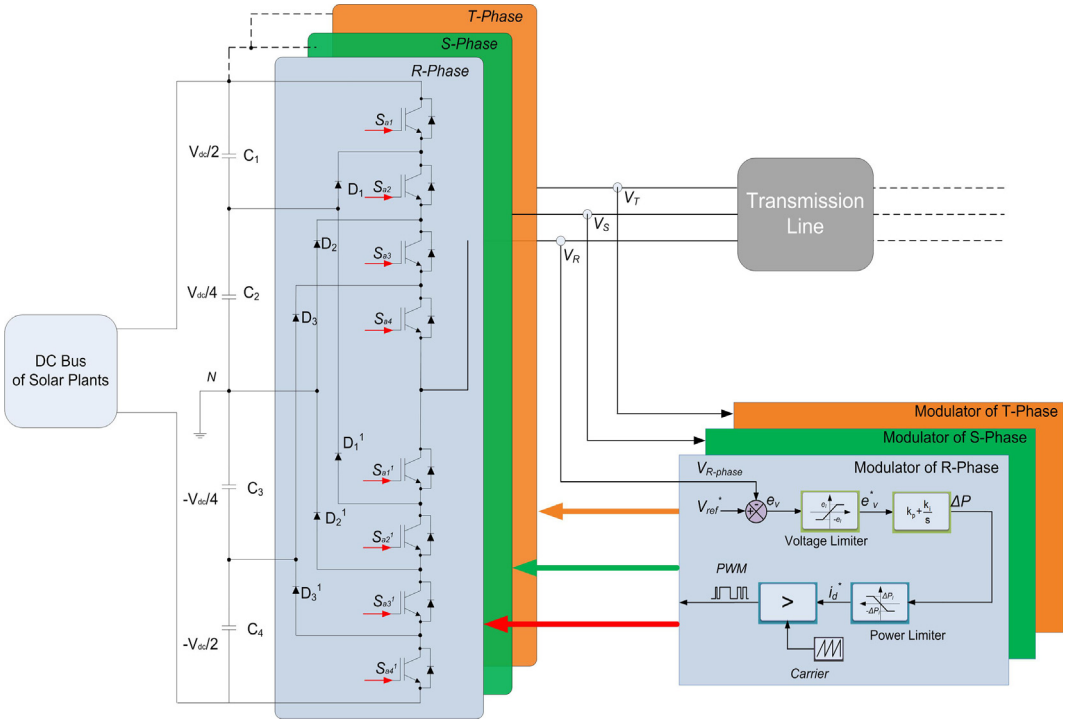

Fig. 4. Multilevel inverter and controllers.

Table 1
Voltage levels of five-level DC-MLI and switching states.

Voltage V_{RN}	Switching state							
	S_{a1}	S_{a2}	S_{a3}	S_{a4}	S_{a1}^{1}	S_{a2}^{1}	S_{a3}^{1}	S_{a4}^{1}
$V_4 = V_{dc}/2$	1	1	1	1	0	0	0	0
$V_3 = V_{dc}/4$	0	1	1	1	1	0	0	0
$V_2 = 0$	0	0	1	1	1	1	0	0
$V_1 = -V_{dc}/4$	0	0	0	1	1	1	1	0
$V_0 = -V_{dc}/2$	0	0	0	0	1	1	1	1

The generated staircase and sinusoidal line voltages of each phase are shown in Fig. 4 that are converted from dc bus voltage seen in Fig. 5. The inverter analyses are performed regarding to varying dc input voltage that is generated by the solar plants operated under various irradiation magnitudes. The voltage levels are kept stable owing to control capacity of modulator, and total harmonic distortion (THD) rates that are observed against various conditions verified the robust structure of controller. The THD analysis of line voltages and load currents are analyzed in the last section.

3. Design of transmission and monitoring stages in the advanced metering infrastructure (AMI) model

The dc-dc conversion realized at the buck converter ensures the stability of the generated energy in each solar plant separately. The acquired dc voltages at the output of the solar farms are collected at the dc bus bar part of the designed system. The output voltage of dc bus bar is fed to diode clamped MLI that is controlled with PD-SPWM to generate three-phase ac line voltages. The length of the transmission line that is introduced in the following subsection is selected as 25 km at the output of the inverter with parameters seen in Table 2.

Table 2
Values of transmission line parameters.

Unit	Value
Length	25 km
Frequency	50 Hz
Resistance	0.2568 Ω/km
Inductance	4×10^{-7} H/km
Capacitance	8.6×10^{-9} F/km

3.1. Transmission section of the system

Three-phase PI section transmission line model is utilized in the designed remote monitoring system. The length of the transmission line is selected as 25 km at the output of the multilevel inverter. In order to determine channel characteristic of the transmission line that will be utilized as a communication medium as well as power delivery, a detailed simulation study is firstly performed in the Advanced Design System (ADS) simulation software. The schematic diagram of the modeled transmission line in ADS software is shown in Fig. 6. When the transmission line modeled, the equivalent of the three-phase PI section line is utilized as can be seen from the figure. The values of the transmission line parameters are determined by using following equations and values

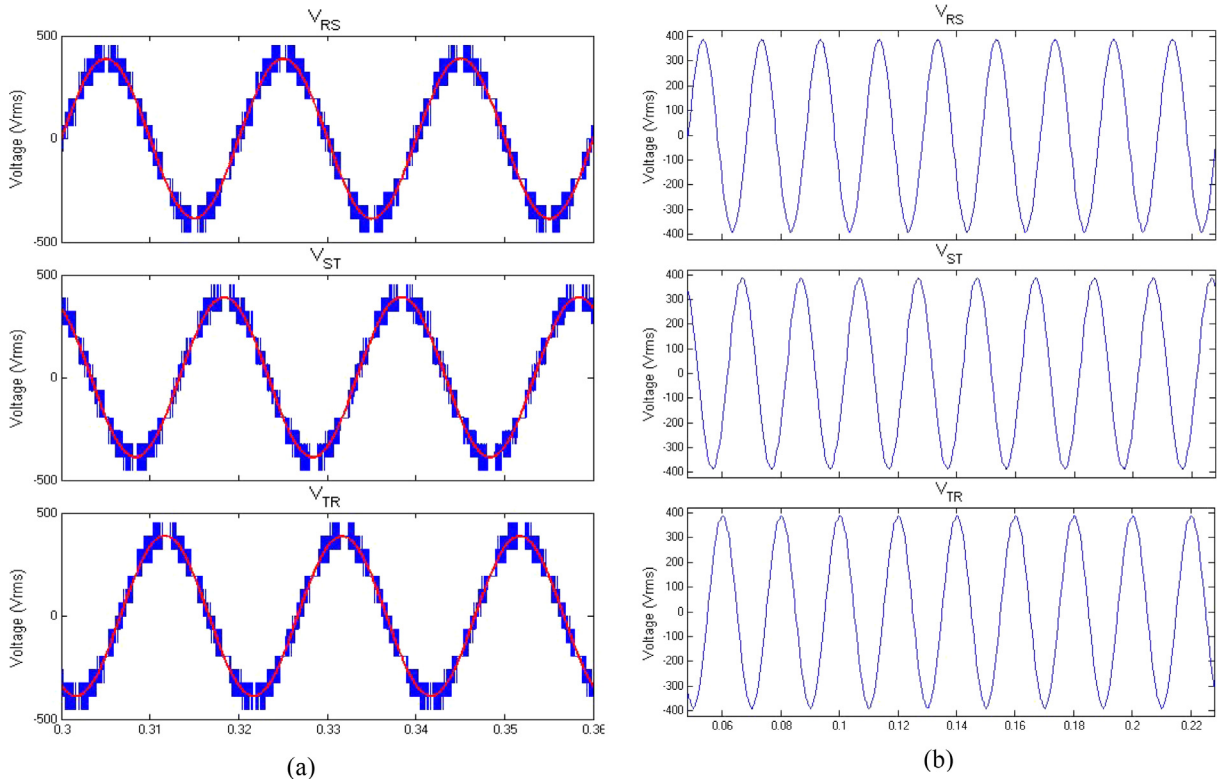

Fig. 5. Multilevel inverter; (a) multilevel and sinusoidal line voltages, (b) line voltages at load node.

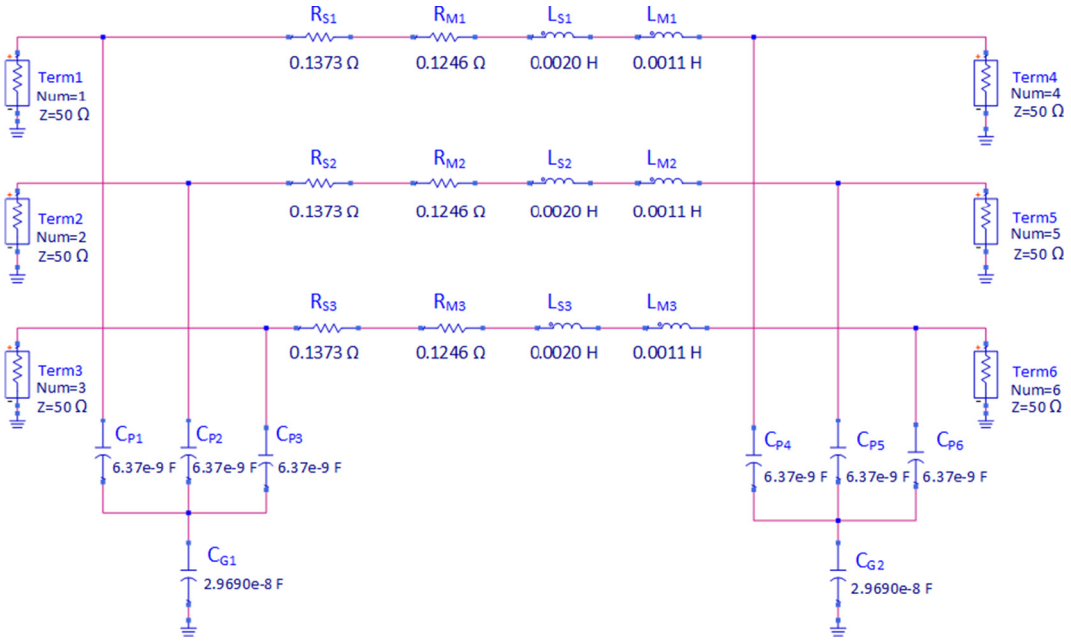

Fig. 6. Modeling of three-phase PI section transmission line in ADS software.

listed in Table 2 that the parameters are calculated regarding to following equations,

$$R_S = \frac{(2R_1 + R_0)}{3}, \quad R_M = \frac{(R_0 - R_1)}{3} \tag{1}$$

$$L_S = \frac{(2L_1 + L_0)}{3}, \quad L_M = \frac{(L_0 - L_1)}{3} \tag{2}$$

$$C_P = C_1, \quad C_G = \frac{3C_1C_0}{(C_1 - C_0)} \tag{3}$$

where while the R_S and R_M denote self-resistance and mutual resistance, L_S and L_M are self-inductance and mutual inductance, respectively. C_P and C_G show phase capacitance and ground capacitance, respectively. The R_0, R_1, L_0, L_1, C_0 and C_1, parameters shown in equations are defined as follows.

$$R_0 = r_0 \cdot l_{length} \cdot k_{r0}, \quad R_1 = r_1 \cdot l_{length} \cdot k_{r1} \tag{4}$$

$$L_0 = l_0 \cdot l_{length} \cdot k_{l0}, \quad L_1 = l_1 \cdot l_{length} \cdot k_{l1} \tag{5}$$

$$C_0 = c_0 \cdot l_{length} \cdot k_{c0}, \quad C_1 = c_1 \cdot l_{length} \cdot k_{c1} \tag{6}$$

where r_1 and r_0 are resistances, l_1 and l_0 are inductances and c_1 and c_0 are capacitances in terms of per unit length and positive- and zero-sequence, respectively.

The l_{length} parameter is length of the transmission line whose value is selected as 25 km as mentioned before. After the transmission line is modeled in the ADS software, simulation studies are performed to obtain characteristics of the transmission line up to 100 kHz frequency. The behavior of the transmission line in case of exploiting as a communication channel medium is acquired as shown in Fig. 7.

When the characteristic is analyzed, it is shown that the transmission line has an increasing attenuation feature with rising frequency value. Therefore, when the communication system is designed, below of the 10 kHz frequency is selected to ensure that the destructive effects of the channel less affect the communication signals.

Two different rated loads are considered in the designed system. While one of the load plants is formed as a 2500 W rated load,

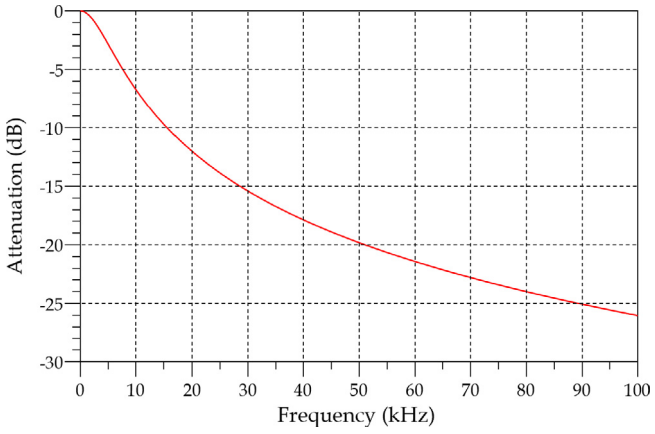

Fig. 7. Characteristic behavior of the transmission line with increasing frequency.

the other is established with 1500 W rated load. Each of the load plants is monitored by designed modems that are separately located and utilized at dissimilar frequencies to convey measured power rate. Different carrier frequencies are selected for mapping multi-channel input data thanks to designed modems at the energy generation part of the system.

In the proposed system, 6 kHz and 8 kHz carrier frequencies are preferred due to two important reasons. One of the reasons is to cope with adjacent channel interference problem while the second reason is to decrease disruptive effects of the transmission medium as mentioned before. Moreover, the designed modems are constructed to recover carrier frequencies accurately. The designed modems can be reconfigured when the numbers of load plants are increased. The monitoring system of the proposed design will be explained in the next section in detail.

3.2. Monitoring section of the system

Communication infrastructure of the system is constituted thanks to BPSK modems that are seen in the Fig. 1. These modems

are very important parts of the proposed monitoring system for conveying and receiving values of measurement. The BPSK modulation scheme is one of the most robust digital scheme against to noise effects. Two different phases that are generally separated by 180° or π radians from each other are employed in this mapping method. Mathematical expression of this mapping technique can be given as

$$s_{BPSK}(t) = \begin{cases} \gamma(t)(A\cos(2\pi f_c t)), & \text{for a data 1} \\ -\gamma(t)(A\cos(2\pi f_c t)), & \text{for a data 0} \end{cases} \quad (7)$$

where A shows amplitude of the carrier signal, $\gamma(t)$ is a random binary pulse with period of T_0 and its level changes between -1 and 1, and f_C is frequency parameter of the carrier signal. When the value of the data is 1 then the phase of the $s_{BPSK}(t)$ signal will be obtained as 0, otherwise the phase degree will be π. Symbol energy (E) of the BPSK signal can be expressed as follows:

$$s_{BPSK}(t) = \begin{cases} \sqrt{\frac{2E}{T_0}}\cos(2\pi f_c t), & \text{for a data 1} \\ -\sqrt{\frac{2E}{T_0}}\cos(2\pi f_c t), & \text{for a data 0} \end{cases} \quad (8)$$

where the symbol energy (E) is equivalent to $E = (\frac{1}{2})A^2 T_0(\gamma(t))^2$ (Xiong, 2000; Glover and Grant, 2000; Harada and Prasad, 2002). Fig. 8a shows the block diagram of the designed modem for one channel case. The modulator scheme of the system is shown at the top of the figure. The power measurement process from the PV panels in real-time is realized by measured power block. Following the measurement process, acquired information is primarily transformed to the digital data. Message signal and carrier signal are usually multiplied to obtain the BPSK waveform. However, this method is not an proper process to generate modulated signal because of the bandwidth issue of real systems. Probability of error at the receiver side is increased due to the limited bandwidth.

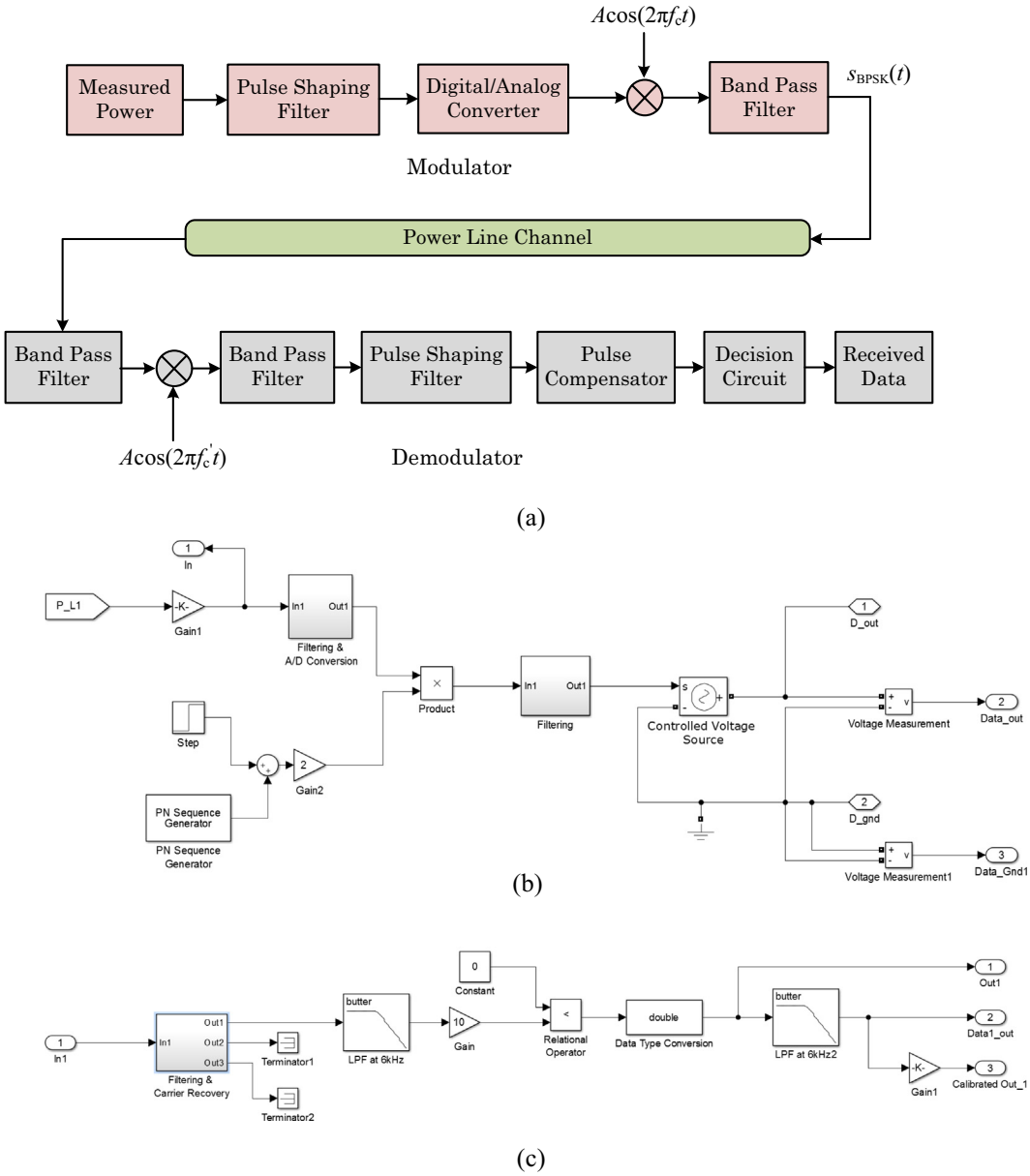

Fig. 8. Communication infrastructure of designed AMI system; (a) Block diagram of the designed PLC modem, (b) developed modulator structure in Matlab/Simulink, (c) demodulator structures designed in Matlab/Simulink.

Pulse-shaping methods are generally exploited at the modulator side before the mapping process to handle this problem. After the pulse-shaping process, data is transformed to the analog signal type by using a digital to analog converter (DAC) block. In the next step, analog signal is multiplied with a sinusoidal carrier signal for mapping process and the modulated signal is applied to a band pass filter (BPF) to limit bandwidth of the signal. After these processes, the signal is fed to the transmission channel in which a power line channel conditions are took into account in the study. The received signal is primarily fed to the BPF filter to separate noises from the received message signal at the receiver part of the system. Following the filtering process, obtained signal is again multiplied with carrier signal for moving it to baseband. Later, different processes such as pulse-shaping, filtering, and pulse compensation techniques are carried out to eliminate inter symbol interference (ISI) effect. In the final step, decision circuit block detects whether the received

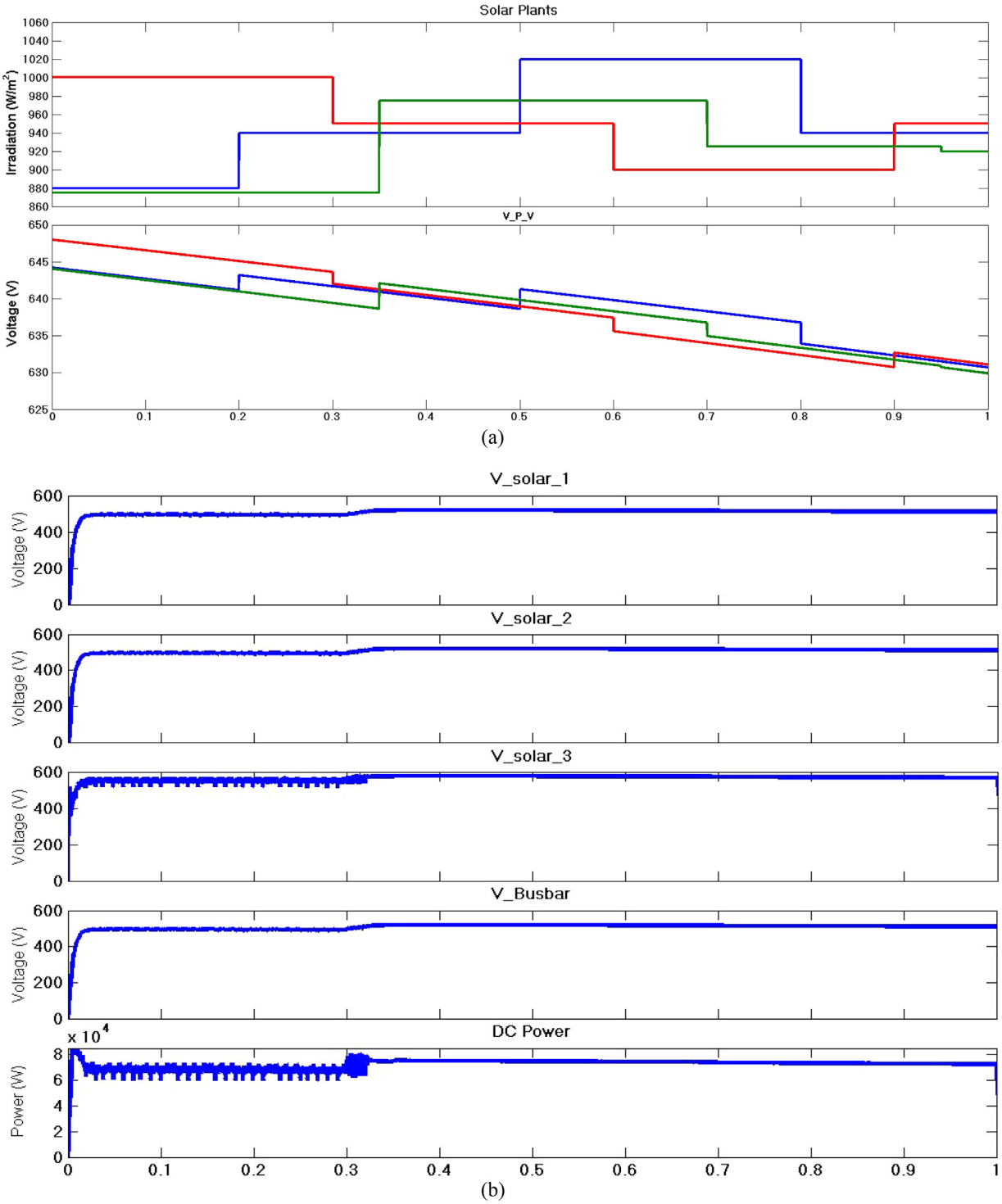

Fig. 9. Solar plant generation analyses, (a) irradiation magnitudes at each solar plant, (b) solar plant output voltage, dc bus voltage, and total output power of the plants.

signal is a zero data or a one data (Xiong, 2000; Glover and Grant, 2000; Harada and Prasad, 2002).

The Simulink implementation of modulator and demodulator structures for one channel case is shown in Fig. 8b and Fig. 8c, respectively. As can be seen from the input of the modulator structure, the measured signal is firstly filtered and transformed digital signal by Filtering & A/D conversion block.

After the mapping process is performed, the modulated signal are filtered and the final message signal is fed to the communication medium. The message signal received by the demodulator system is firstly filtered to reduce destructive effects of the channel and then carrier recover procedure is performed. In addition, demodulation process is also realized at the Filtering & Carrier Recovery block. After these processes are conducted, pulse shaping and decision processes are carried out at the demodulator structure, respectively. At the demodulator structure, a fourth order filter is utilized to obtain appropriate results. The results of the modulator and demodulator systems will be presented by the following section.

4. Comprehensive performance analysis of the proposed system

The designed monitoring system is examined in terms of generation and energy conversion section, transmission/monitoring section and microgrid load section as mentioned previously. The dc voltages generated at solar plants of energy generation part are delivered to the bus bar over the interphase transformers in order to keep the total dc voltage at a fixed value. The solar plants are tested under various irradiation conditions as shown in Fig. 9a where the irradiations are arbitrarily changed to analyze the success of dc converter and coupled operation on dc busbar. The irradiations applied to 1st solar plant is get varied as an index of [880 940 1020 940] W/m^2 at [0 0.2 0.5 0.8] second intervals as

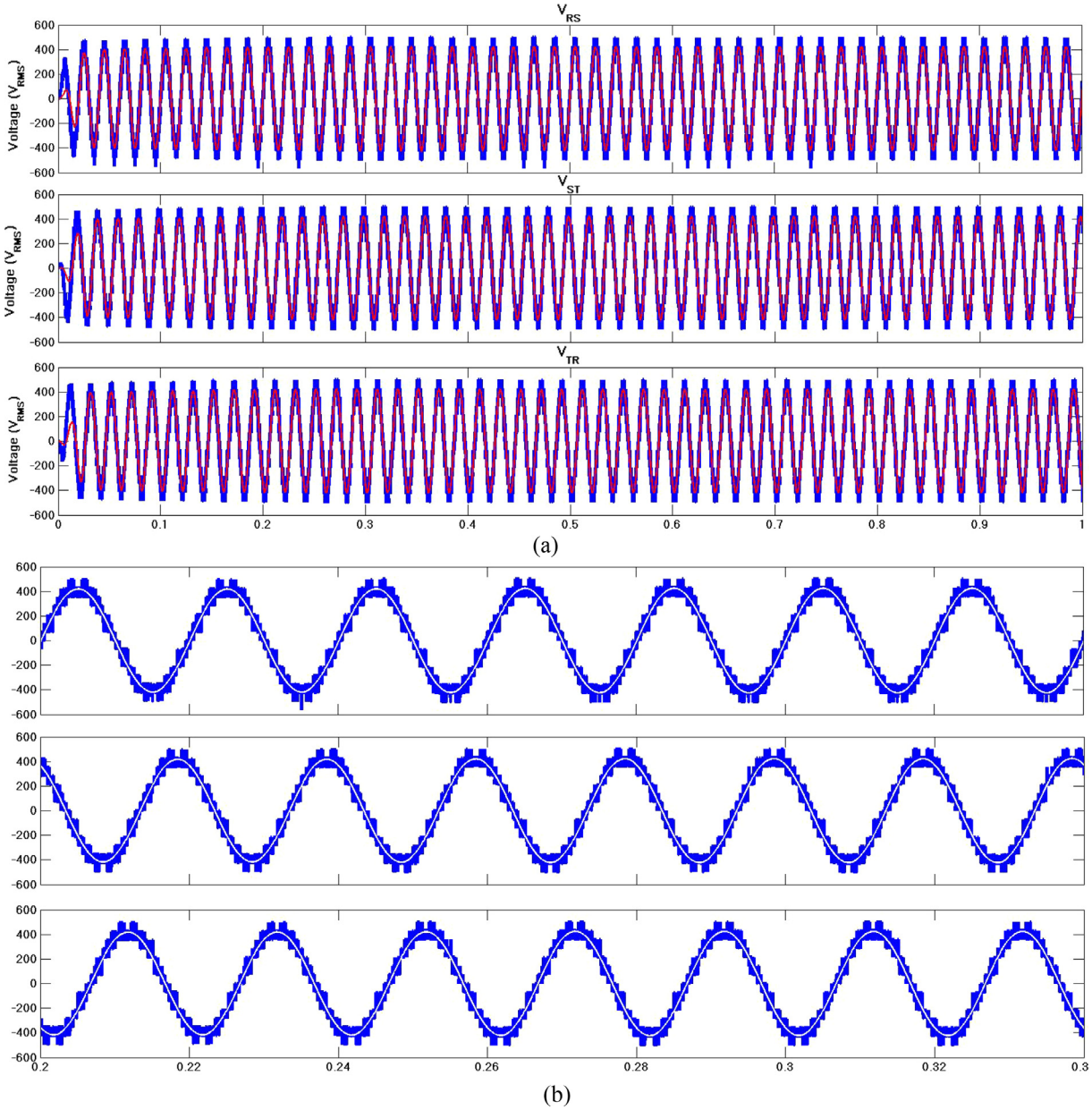

Fig. 10. Energy conversion section analyses, (a) line voltages at MLI output, (b) staircase and sinusoidal MLI voltages.

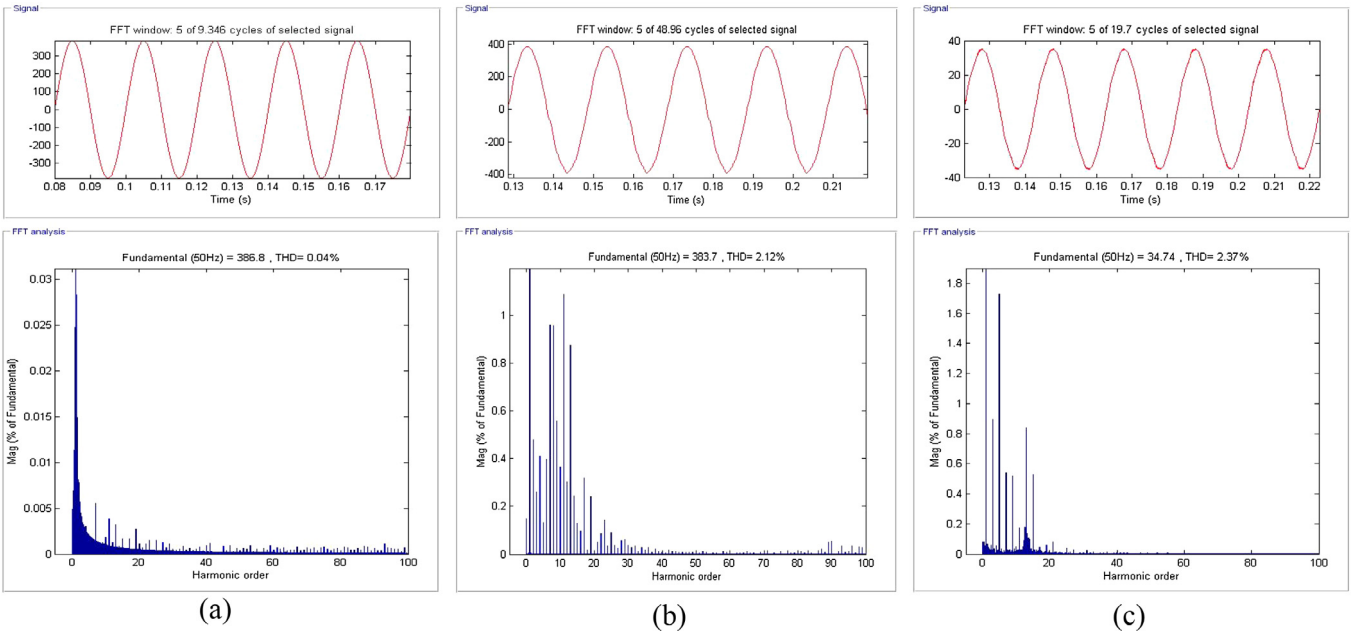

Fig. 11. Energy conversion section THD analyses, (a) line voltages THD at unloaded operation, (b) line voltages THD at fully loaded operation, (c) line current THD at loaded operation.

depicted with the blue line. The corresponding dc output voltage of solar plant is shown in the second curve of Fig. 9a by blue line as in irradiation curve. The irradiation index and intervals of 2nd plant are as [1000 950 900 950] W/m^2 and [0 0.3 0.6 0.9] s depicted with red line, and the corresponding output voltage variation is shown by red line on second curve of Fig. 9a. The 3rd solar plant where the irradiation and output voltages are shown with green lines is tested by [875 975 925 920] W/m^2 irradiation index changing at [0 0.35 0.7 0.95] s. The MPPT algorithm limits the effect of the irradiation change that causes around 5 V fluctuation at the output voltage of solar arrays. On the other hand, the dc converters regulate the output voltages of each solar plant to ensure the dc busbar to provide stable voltage to MLI.

The regulated output voltage of each solar plant and dc busbar voltage where all the solar plants are coupled are illustrated in Fig. 9b where the supplied dc power to the full loaded analyze are shown in the last curve. The MPPT algorithms used in the control of dc buck converters are responsible to provide available maximum output power to the energy conversion section comprised by the MLI inverter. Furthermore, the regular MPPT algorithm based on Perturb and Observe approach that many surveys can be found in the literature limits the output voltage in a hysteresis band of 480–520 V. The first voltage curve seen on Fig. 9b belong to the output voltage of Solar Plant #1 that the irradiation and solar array output voltages are shown with blue lines in Fig. 9b.

The second curve belongs to Solar Plant #2 that the irradiation and solar array output voltages are red lines in Fig. 9a while the third curve is the resultant voltage of Solar Plant #3 where the array voltage and irradiations are shown with green line in Fig. 9a. The solar plant output voltages and dc bus voltage fluctuates around 490–500 V up to 0.3 s interval since all the plant irradiations are independently varied where the first and third plant irradiations were real lower than 1000 W/m^2 of 2nd plant. The dc bus voltage ripple was around ±5 V on 490 V during these circumstances. Once the irradiation of 2nd plant increased from 875 W/m^2 to 975 W/m^2 at 0.35 s, the rough fluctuation seen on 3rd curve of Fig. 9b is decreased and the power fluctuation seen in the last curve is easily regulated by the dc converters. The following variations are not significantly effective on regulated voltage and power since they were higher than 900 W/m^2.

The MLI output voltages are analyzed under various irradiations of solar plants that are presented above. The measurement results of staircase and sinusoidal V_{RS}, V_{ST}, and V_{TR} line voltage are shown in Fig. 10a. Since regular PI controller independently manages each phase voltages as shown in Fig. 4, effects of the dc voltage fluctuations seen on Fig. 9b are compensated at the phase outputs of MLI. Although there some increases seen at 0.45 s and 0.7 s, the most significant fluctuations of dc voltages occurred up to 0.3 s are eliminated at the output of MLI. The detailed view of staircase and sinusoidal voltages are presented in Fig. 10b where the line voltages are at 380 V_{RMS} and frequencies at 50 Hz. The quality of line voltages at unloaded and fully load conditions, and line current at loaded operations are analyzed in Fig. 11a–c respectively.

Fig. 11a presents the line voltage THD analysis while MLI is operated without any load. The measured THD ratio at this analysis is 0.04% where almost all the baseband and carrier harmonics are eliminated. While MLI is fully loaded with 75 kW resistive and inductive load, the line voltage is decreased from 386.8 V to 383.7 V and the THD of line voltage is increased to 2.12% (Fig. 11b) where 5th, 7th, 9th, 11th ordered harmonics that are assumed as the most significant ones are lower than 1%. In another measurement, the MLI is loaded with 13 kW resistive and inductive load and current THD analysis is performed where the resultant THD is at 2.37% as seen in Fig. 11c.

The transmission line is employed to deliver power load plants that are different and with dissimilar power consumption features. The first plant presented in the lower part of the microgrid load side is constructed for consuming approximately 2500 W while the second one expends about 1500 W. The power consumption values of the plants are acquired by the designed wattmeter. Figs. 12 and 13 depict obtained analysis results for the examined loads, respectively. Each one of the load plants contains a modem that can quantize the detected power consumption and mapping the data which will be conveyed to transmission line as a transmis-

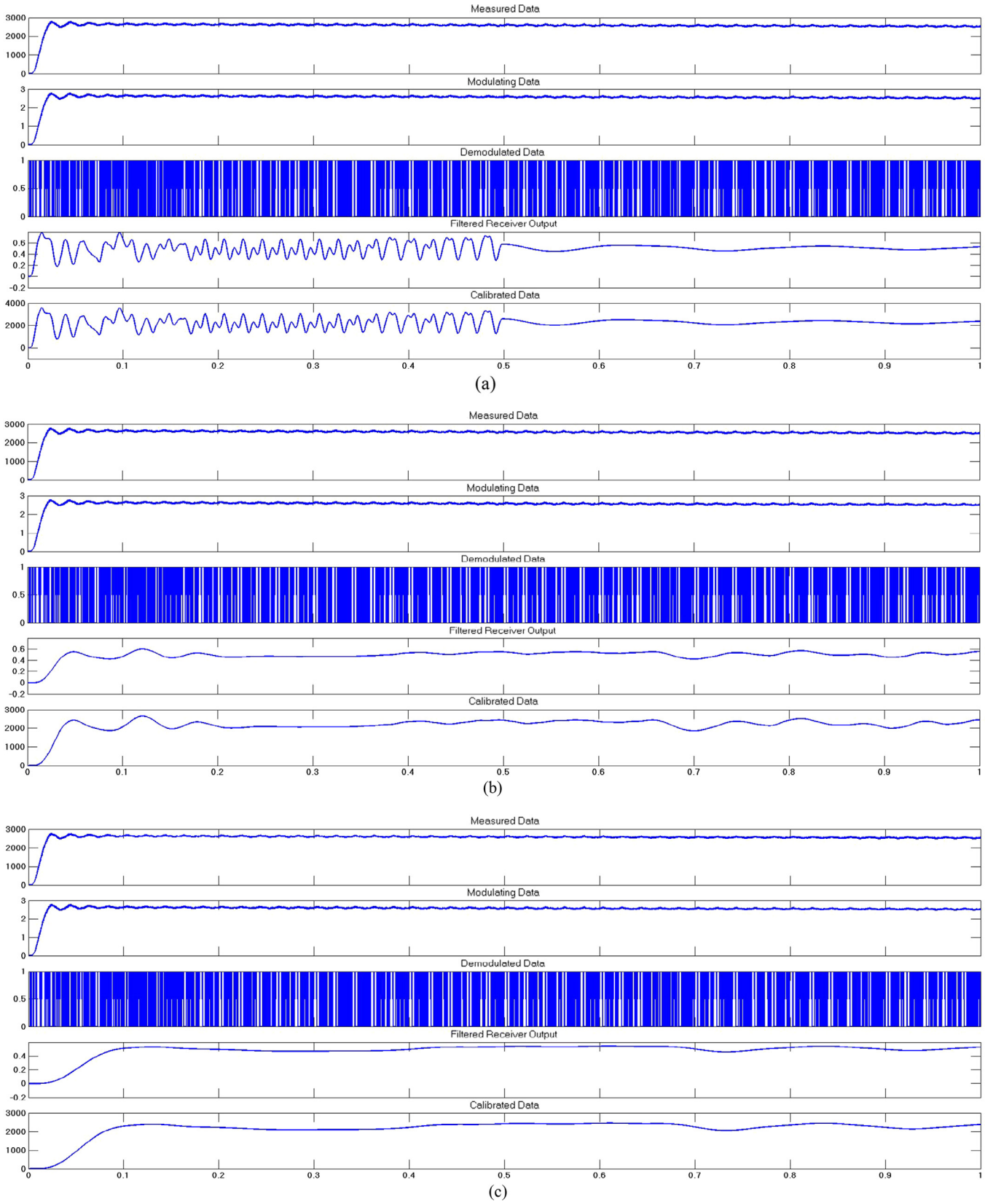

Fig. 12. Transmitted, demodulated and calibrated signals of first load plant, (a) filtering at 400 Hz 2nd order, (b) filtering at 200 Hz 2nd order, (c) filtering at 50 Hz 4th order.

sion medium. The measured power consumptions of each load plant are presented in the first axis of the Figs. 12 and 13, respectively. As can be seen in the second axis of the figures, the measured data are transformed to mapping data in modulator system by attenuating at a rate of 1:1000. While the mapping data of the first plant is mapped by a carrier signal at 8 kHz frequency,

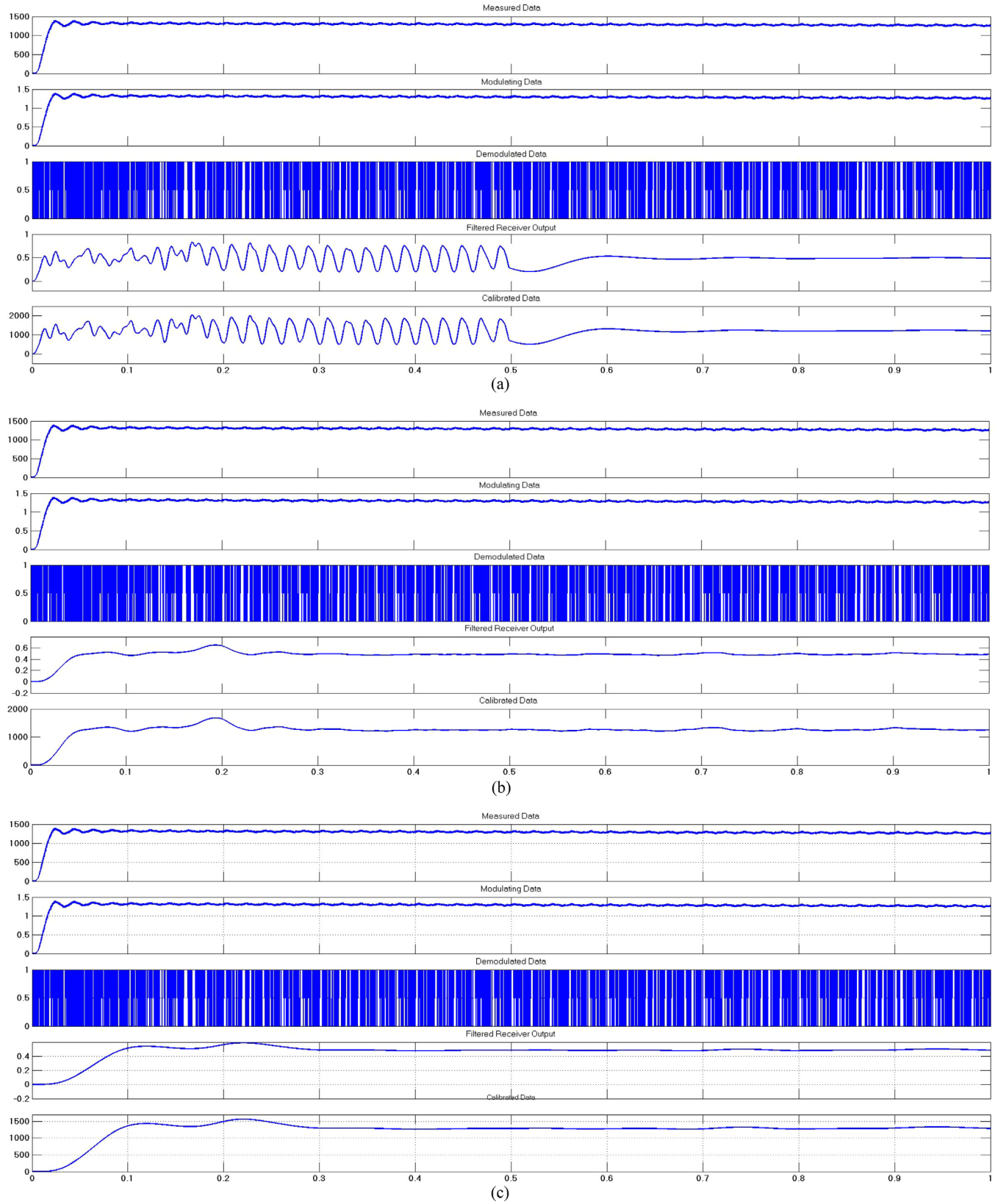

Fig. 13. Transmitted, demodulated and calibrated signals of second load plant, (a) filtering at 400 Hz 2nd order, (b) filtering at 200 Hz 2nd order, (c) filtering at 50 Hz 4th order.

the other one is mapped by a carrier signal at 6 kHz frequency. The filtering analyses are performed by adjusting the filter order and cut-off frequency at 400 Hz 2nd order, 200 Hz 2nd order, and 50 Hz 4th order in Fig. 12a–c respectively for the first load plant while second plant analyses are shown in Fig. 13a–c under same circumstances.

The monitoring modem that is placed at the output of the diode clamped multilevel inverter is also associated with a coupling circuit similar to utilized at the modulator side. The decreased line voltage with mapped data is applied to the demodulator system and is passed a filter to clear harmonic contents at the output of the demodulator. The demodulator part of the designed modem placed in the monitoring side is constituted to acquire carrier signals at 6 kHz and 8 kHz frequencies to choose plant data severally. The demodulated message signal are presented in the third axis of the Figs. 12 and 13 that are obtained by filtering a fourth order low-pass Butterworth filters. In addition, carrier signal recoveries of the demodulators contain band-pass filters with ±100 Hz lower and upper band edge frequencies. Besides, output filters of the demodulator systems are adjusted to 50 Hz pass band edge frequency to suppress the line voltages. Following the filtering process, calibrating process is applied to determine real-time power consumption values in terms of watt. While the obtained receiver outputs after filtering process are illustrated in the fourth axis of the Figs. 12 and 13, the calibrated outputs are depicted in the last axis of figures. The measured and monitored power signals of the examined microgrid are considered, it is clear that designed monitoring system can be efficiently utilized to monitor renewable energy sources placed in different locations.

5. Conclusion

The observing and metering processes are necessary in renewable energy conversion systems as applied in smart grid applications of conventional grid. A microgrid model including separate solar and load plants is established and is comprehensively examined in this study. The electricity generation part of the modeled microgrid contains three solar plants that are supposed to be placed in different locations. The solar plants are configured with 150 PV modules each at 170 Wp rated power, and generated solar array voltages are regulated by buck converters to supply a diode clamped MLI around 500 V. The buck converters are controlled by using regular P&O MPPT algorithm that ensures to acquire the maximum available power and regulated dc output voltage at the desired magnitude. On the other hand, the diode clamped MLI, which is a convenient alternative to conventional full bridge inverter topology in terms of requiring a single dc voltage source, and robustly decreasing the current and voltage THD ratios, is operated by PD-SPWM modulation scheme with independent phase control that enforces the inverter against unbalanced loads. This topic is planned to be researched in the future studies. The transmission and distribution model of presented microgrid system is designed with realistic impedance values of a 25 km transmission line, and the configured line is utilized as the communication medium in addition to carrying power. The distribution line section is constituted with two load plants where the power consumptions of the load plants are measured and are mapped by the designed modem to realize the PLC infrastructure. The carrier frequencies are set to 6 kHz and 8 kHz for any load plant, and thus the communication channels on the power line are obtained. The acquired results clearly confirm that the installation costs of remote monitoring systems, which are necessary in the SCADA, wireless communication systems or in any Ethernet-based systems, are removed thanks to the proposed monitoring system. In addition, the number of the load plants can be easily augmented by employing the proposed monitoring system in the possible future works.

References

Ahmed, M.A., Pan, J.-K., Song, M., Kim, Y.-C., 2016. Communication network architectures based on ethernet passive optical network for offshore wind power farms. Appl. Sci. 6 (3), 81.

Almas, M.S., Vanfretti, L., Løvlund S., Gjerde, J.O., Open source SCADA implementation and PMU integration for power system monitoring and control applications, In: 2014 IEEE PES General Meeting|Conference & Exposition, 2014, pp. 1–5.

Atalik, T. et al., 2014. Multipurpose platform for power system monitoring and analysis with sample grid applications. IEEE Trans. Instrum. Meas. 63 (3), 566–582.

Cabanas, M.F. et al., 2007. A new online method based on leakage flux analysis for the early detection and location of insulating failures in power transformers: application to remote condition monitoring. IEEE Trans. Power Deliv. 22 (3), 1591–1602.

Chi, H.R., Tsang, K.F., Chui, K.T., Chung, H.S.H., Ling, B.W.K., Lai, L.L., 2016. Interference-mitigated ZigBee-based advanced metering infrastructure. IEEE Trans. Ind. Inf. 12 (2), 672–684.

Çolak, I., Kabalcı, E., Bayındır, R., 2011. Review of multilevel voltage source inverter topologies and control schemes. Energy Convers. Manage. 52, 1114–1128.

Collotta, M., Pau, G., 2015. A novel energy management approach for smart homes using bluetooth low energy. IEEE J. Sel. Areas Commun. 33 (12), 2988–2996.

Fabrizio, E. et al., 2017. Monitoring and managing of a micro-smart grid for renewable sources exploitation in an agro-industrial site. Sustain. Cities Soc. 28, 88–100.

Fateh, B., Govindarasu, M., Ajjarapu, V., 2013. Wireless network design for transmission line monitoring in smart grid. IEEE Trans. Smart Grid 4 (2), 1076–1086.

Gaurav, D., Mittal, D., Vaidya, B., Mathew, J. A GSM based low cost weather monitoring system for solar and wind energy generation, In: The Fifth International Conference on the Applications of Digital Information and Web Technologies (ICADIWT 2014), 2014, pp. 1–7.

Ginot, N., Mannah, M.A., Batard, C., Machmoum, M., 2010. Application of power line communication for data transmission over PWM network. IEEE Trans. Smart Grid 1 (2), 178–185.

Glover, I., Grant, P., 2000. Digital Communications. Prentice Hall, Great Britain.

Harada, H., Prasad, R. Simulation and software radio for mobile communication, Artech House Publishers, 2002.

Harid, N., Bogias, A.C., Griffiths, H., Robson, S., Haddad, A., 2016. A wireless system for monitoring leakage current in electrical substation equipment. IEEE Access 4, 2965–2975.

Kabalci, E., 2013. Design and analysis of a hybrid renewable energy plant with solar and wind power. Energy Convers. Manage. 72, 51–59.

Kabalci, E., 2015. A smart monitoring infrastructure design for distributed renewable energy systems. Energy Convers. Manage. 90, 336–346.

Kabalci, E., Kabalci, Y., BPSK modem based power line communication system for observing photovoltaic panels, In: Presented at the 2nd International Conference on Nuclear and Renewable Energy Resources (NURER 2010), Ankara, Turkey, July 4–7, 2010, 2010.

Kabalci, E., Kabalci, Y., Develi, I., 2012. Modelling and analysis of a power line communication system with QPSK modem for renewable smart grids. Int. J. Electr. Power Energy Syst. 34 (1), 19–28.

Kabalci, Y., Kabalci, E., Canbaz, R., Calpbinici, A., 2016. Design and implementation of a solar plant and irrigation system with remote monitoring and remote control infrastructures. Sol. Energy 139, 506–517.

Kamel, T., Biletskiy, Y., Chang, L., 2015. Fault diagnosis and on-line monitoring for grid-connected single-phase inverters. Electr. Power Syst. Res. 126, 68–77.

Kosonen, A., Ahola, J., 2010. Comparison of signal coupling methods for power line communication between a motor and an inverter. IET Electr. Power Appl. 4 (6), 431–440.

Kurohane, K., Senjyu, T., Yona, A., Urasaki, N., Goya, T., Funabashi, T., 2010. A hybrid smart AC/DC power system. IEEE Trans. Smart Grid 1 (2), 199–204.

Le, P.T., Tsai, H.-L., Lam, T.H., 2016. A wireless visualization monitoring, evaluation system for commercial photovoltaic modules solely in MATLAB/simulink environment. Sol. Energy 140, 1–11.

Lin, C.K., Lu, M.T., Yeh, S.C., Chen, H.H., 2009. Video streaming over in-home power line networks. IEEE Trans. Multimedia 11 (3), 523–534.

Ma, T., Yang, H., Lu, L., 2013. Performance evaluation of a stand-alone photovoltaic system on an isolated island in Hong Kong. Appl. Energy 112, 663–672.

Madueño, G.C., Nielsen, J.J., Kim, D.M., Pratas, N.K., Popovski, P., 2016. Assessment of LTE wireless access for monitoring of energy distribution in the smart grid. IEEE J. Sel. Areas Commun. 34 (3), 675–688. S. Č.

Mannah, M.A., Batard, C., Ginot, N., Machmoum, M., 2011. A PLC-based method for data transmission over a pulsewidth-modulated network. IEEE Trans. Power Deliv. 26 (4), 2259–2266.

Mohamed, F.P., Siew, W.H., Soraghan, J.J., Strachan, S.M., Mcwilliam, J., 2014. Remote monitoring of partial discharge data from insulated power cables. IET Sci. Meas. Technol. 8 (5), 319–326.

Padilla, E., Agbossou, K., Cardenas, A., 2014. Towards smart integration of distributed energy resources using distributed network protocol over ethernet. IEEE Trans. Smart Grid 5 (4), 1686–1695.

Senthilnathan, K., Annapoorani, I., 2016. Implementation of unified power quality conditioner (UPQC) based on current source converters for distribution grid and performance monitoring through LabVIEW Simulation Interface Toolkit server: a cyber physical model. IET Gen. Transm. Distrib. 10 (11), 2622–2630.

Shariff, F., Rahim, N.A., Ping, H.W., 2013. Photovoltaic remote monitoring system based on GSM. IEEE Conference on Clean Energy and Technology (CEAT) 2013, 379–383.

Shariff, F., Rahim, N.A., Hew, W.P., 2015. Zigbee-based data acquisition system for online monitoring of grid-connected photovoltaic system. Expert Syst. Appl. 42 (3), 1730–1742.

Sharp NE-170UC1 Multipurpose Module, Sharp, USA, 2008. Available at: http://files.sharpusa.com/Downloads/Solar/Products/sol_dow_NE170U1.pdf.

Silva, A.S., dos Santos, R.C., Bottura, F.B., Oleskovicz, M., 2017. Development and evaluation of a prototype for remote voltage monitoring based on artificial neural networks. Eng. Appl. Artif. Intell. 57, 50–60.

Silvestre, S., Chouder, A., Karatepe, E., 2013. Automatic fault detection in grid connected PV systems. Sol. Energy 94, 119–127.

Son, Y., Pulkkinen, T., Moon, K.d., Kim, C., 2010. Home energy management system based on power line communication. IEEE Trans. Consum. Electron. 56 (3), 1380–1386.

Tina, G.M., Grasso, A.D., 2014. Remote monitoring system for stand-alone photovoltaic power plants: the case study of a PV-powered outdoor refrigerator. Energy Convers. Manage. 78, 862–871.

Tsuzuki, S., 2006. High-speed power-line communication and its application to a localization system. IEICE Trans. Fundament. Electron. Commun. Comput. Sci. E89A (11), 3006–3012.

Tung, H.Y. et al., 2014. The generic design of a high-traffic advanced metering infrastructure using zigbee. IEEE Trans. Ind. Inf. 10 (1), 836–844.

Vanfretti, L., Baudette, M., Domínguez-García, J.-L., Almas, M.S., White, A., Gjerde, J. O., 2016. A phasor measurement unit based fast real-time oscillation detection application for monitoring wind-farm-to-grid sub–synchronous dynamics. Electr. Power Comp. Syst. 44 (2), 123–134.

Venkatraman, K., Reddy, B.D., Selvan, M.P., Moorthi, S., Kumaresan, N., Gounden, N. A., 2016. Online condition monitoring and power management system for standalone micro-grid using FPGAs. IET Gen. Transm. Distrib. 10 (15), 3875–3884.

Wilkinson, M., Darnell, B., Delft, T.V., Harman, K., 2014. Comparison of methods for wind turbine condition monitoring with SCADA data. IET Renew. Power Gen. 8 (4), 390–397.

Xiong, F., 2000. Digital Modulation Techniques. Artech House, USA.

Zaker, N., Kantarci, B., Kantarci, M.E., Mouftah, H.T., 2014. Smart grid monitoring with service differentiation via EPON and wireless sensor network convergence. Optical Switching and Networking 14 (1), 53–68.

Zhang, P., Li, F., Bhatt, N., 2010. Next-generation monitoring, analysis, and control for the future smart control center. IEEE Trans. Smart Grid 1 (2), 186–192.